Estuarine, Coastal and Shelf Science 213 (2018) 283–293

Contents lists available at ScienceDirect

Estuarine, Coastal and Shelf Science

journal homepage: www.elsevier.com/locate/ecss

Intra-annual variability of phytoplankton biomass and nutrients in a tropical estuary during a severe drought

Hortência de Sousa Barroso[a,*], Tallita Cruz Lopes Tavares[a], Marcelo de Oliveira Soares[a,b], Tatiane Martins Garcia[a], Brenda Rozendo[a], Alanne Simone Cavalcante Vieira[a], Patrícia Barros Viana[a,c], Thalita Melo Pontes[a], Tasso Jorge Tavares Ferreira[a], Jurandir Pereira Filho[d], Carlos Augusto França Schettini[e], Sandra Tédde Santaella[a]

[a] Instituto de Ciências do Mar (LABOMAR), Universidade Federal do Ceará, Av. da Abolição, 3207, Meireles, 60165-081, Fortaleza, CE, Brazil
[b] Institut de Ciència i Tecnologia Ambientals (ICTA), Universitat Autònoma de Barcelona (UAB), Edifici Z, 081093, Barcelona, Spain
[c] Universidade Federal do Ceará, Campus Russas, Rua Felipe Santiago, 411, Cidade Universitária, Russas, CE, Brazil
[d] Escola do Mar, Ciência e Tecnologia (EMCT), Universidade do Vale do Itajaí, Rua Uruguai, 458, 88302-901, Itajaí, SC, Brazil
[e] Departamento de Oceanografia, Universidade Federal de Pernambuco, Av. Prof. Moraes Rego, 1235, Cidade Universitária, 50670-901, Recife, PE, Brazil

ARTICLE INFO

Keywords:
Hypersalinity
Chlorophyll
Water budget
Environmental factors
River discharge
Semi-arid

ABSTRACT

This study describes the intra-annual variability of environmental characteristics, hydrologic regime and their potential consequences for phytoplankton biomass in a low-inflow estuary on the Brazilian semi-arid coast. The estuary was subjected to two conditions based on the water and salt balance: a short hyposaline and a long hypersaline period. They were marked by considerable differences in precipitation, evaporation and water flushing time that resulted in noticeable variations in the salinity gradients, nutrient concentrations and total phytoplankton biomass (TPB). TPB peaked at the middle and end of the dry season, when salinity reached maximum levels (up to 63) and the water residence time was higher. Higher TPB was also related to a decline in inorganic nitrogen due to phytoplankton uptake and a decline in water transparency due to phytoplankton shading. Rainfall rather than drought constituted a disturbance for the phytoplankton as TPB declined in the rainy period despite available nutrients. Given the prevalent climate change, increases are predicted in the frequency and intensity of droughts and salinity in estuaries. Although the phytoplankton community seemed adapted, the limits of its adaptability and the effects of hypersalinity should be further evaluated.

1. Introduction

Estuaries are transitional ecosystems characterized by strong environmental gradients in small spatial and temporal scales (Pereira-Filho et al., 2001; Azhikodan and Yokoyama, 2016), in which many species survive and on which we depend (Uddin et al., 2013; Costanza et al., 2014). Nevertheless, they are subjected to multiple natural and human-driven impacts that are intensified by global climate change (Godoy and Lacerda, 2015; Cloern et al., 2016; Schettini et al., 2017). In particular, arid zones are projected by the Intergovernmental Panel on Climate Change (IPCC) to have large temperature increases, rainfall anomalies and more frequent/intense dry spells and droughts (IPCC, 2014; Robins et al., 2016; Marengo et al., 2017a).

Estuaries are important because of their roles in biogeochemical cycling and material transfer in the continent-ocean interface (Bauer et al., 2013). In semi-arid conditions, estuaries experience a strong climate duality in which the freshwater discharge during rainy season can be thirty-fold higher than that in dry season (Molisani et al., 2006). In dry seasons, extended droughts result in a hydrological deficit, which is made worse by water impoundment in drainage basins to store water for human use (Frota et al., 2013). Therefore, many estuaries experience negative water budgets when the evaporation rate is greater than the freshwater flow, and it causes a net inflow of seawater to the atmosphere to compensate for water loss, which results in hypersaline conditions (salinity higher than that in coastal waters) (Largier, 2010). Such scenarios can become extremely common especially in relatively small volume and short length estuaries due to the changing climate trends in arid and semi-arid lands. Low precipitation and high evaporation regions constitute a distinct biotope where adapted species may flourish in the absence of competition (Nche-Fambo et al., 2015; Hemraj et al., 2017).

Such estuaries are commonly found in the semi-arid coasts

* Corresponding author.
E-mail addresses: hortenciasb@yahoo.com.br, hortenciasba@gmail.com (H.d.S. Barroso).

https://doi.org/10.1016/j.ecss.2018.08.023
Received 29 November 2017; Received in revised form 4 August 2018; Accepted 18 August 2018
Available online 23 August 2018
0272-7714/ © 2018 Elsevier Ltd. All rights reserved.

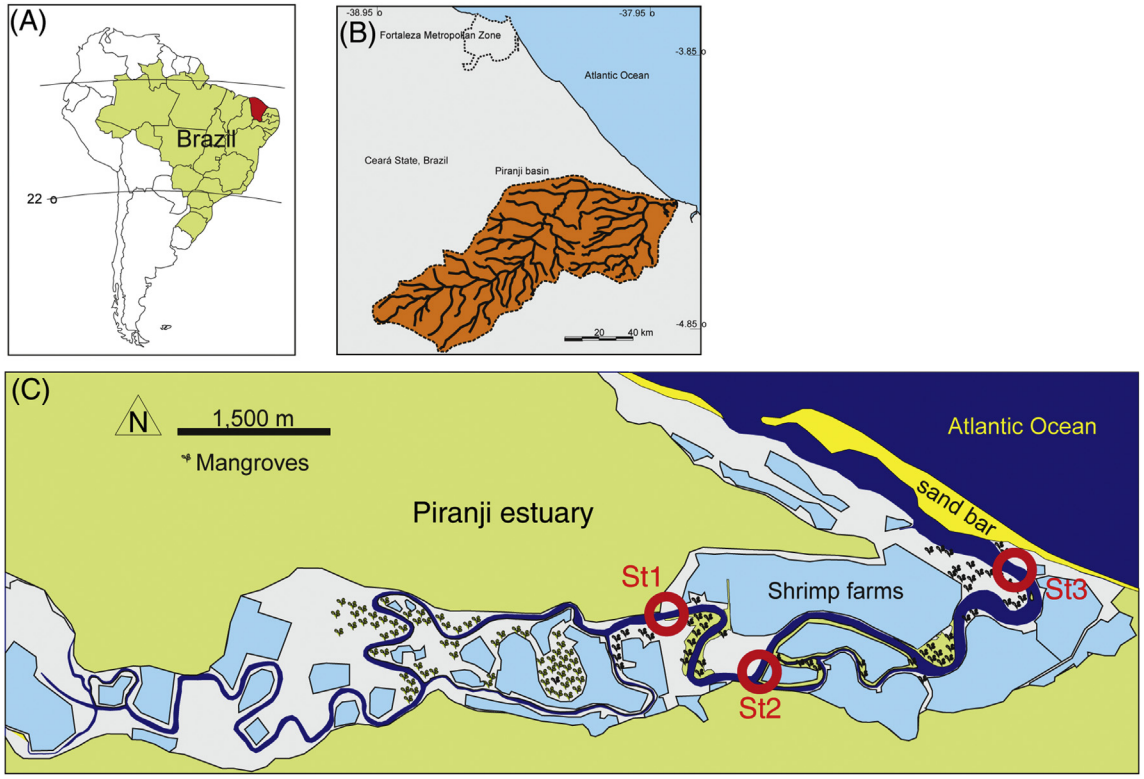

Fig. 1. The locations of sampling sites in the Piranji estuary (CE, northeast Brazil). Ceará State and Drainage basin are shown in red (A) and orange (B).

(Molisani et al., 2006; Valle-Levinson and Schettini, 2016; Schettini et al., 2017). A global trend of increasing water impoundment and worsened climate scenarios may cause more estuaries to experience hypersalinity. Understanding how intensifying droughts could affect the functioning of estuaries is needed to determine the responses of estuaries to these conditions. Thus, here we describe the environmental characteristics and hydrological regime of a relatively small, low-inflow estuary, and we evaluated the potential consequences of drought on phytoplankton biomass. This study was performed in 2015, which allowed us to make observations in an especially severe dry condition (Marengo et al., 2017b). Our study aims to contribute to improve the understanding of human and climate related impacts and the estuarine phytoplankton adaptations to these factors.

2. Material and methods

2.1. Study area

We chose the Piranji river estuary located in the semi-arid coast of Brazil (the northeastern region, 04°23′59″ S, 37°49′18″ W) (Fig. 1) to study the drought effects on the environmental conditions and primary productivity in shallow and short estuaries. The Piranji estuary is ~20 km long and its mean depth is ~3 m, making it a good field laboratory to assess the processes addressed in this study, and providing a model for other low-inflow estuaries. The regional coastal climate is semi-arid warm, with rainy (January to June) and dry (July to December) seasons. It is subjected to very high evaporation rates in an inverted pattern relative to the rainfall (i.e., lower rates from February to June, and higher rates between August and October) (Campos and Studart, 2003). Precipitation and evaporation are influenced locally by orographic rains and humidity blockage, and regionally by Atlantic dipole and El Niño Southern Oscillation (ENSO) (Santos and Brito, 2007). Estimates based on the drainage basin indicate a river discharge approx. 15 m^3/s during the rainy season and < 1 m^3/s in the dry period (Molisani et al., 2006). The precipitation rate is approx. < 1200 mm/year at the coast and < 700 mm/yr inland, and evaporation rate can exceed 1900 mm/year (Uvo and Berndtsson, 1996; Schettini et al., 2017). Although many human activities occur in the Piranji, shrimp farming stands out as the greatest cause of human impacts because of an intense use of natural resources (Meireles et al., 2007). Additionally, Piranji system has multiple dams which were recognized as important regulators of its circulation and transport (Schettini et al., 2017).

2.2. Sampling strategy

Single replicate samples were taken bimonthly on sub-surface (50 cm below water surface) and bottom (25 cm above the bottom) from water column during 2015 from February to December at spring tide in three stations (St1, St2, and St3) along the estuary during ebb tide (Fig. 1c). This tidal stage was chosen to guarantee the sampling of estuarine waters rather than a coastal water parcel advected into the estuary during flood. Samples were maintained at 4 °C after collection and afterwards were subsampled to determination of nutrients, total suspended solids and phytoplankton pigments. Salinity, temperature (T), pH, saturation oxygen (SO) and dissolved oxygen (DO) were measured *in situ* with a multi-parametric probe (YSI 6920 V2) throughout the water column, and the values taken at the sub-surface and near to the bottom were used in this study. Water transparency was estimated with a Secchi disk and the euphotic zone (Z_{eu}) was estimated as 2.7 times the Secchi depth (Cole, 1983). Detailed location information is presented in Supplementary Table S1.

2.3. Samples analyses

Aliquots (1 L) of the water samples were filtered in triplicate through 0.7-μm-pore size glass-fiber filters (47-mm diameter, type GF-3, Macherey-Nagel, Düren, Germany) in less than 8 h after the sampling. The contents of nitrite (NO_2^--N), nitrate (NO_3^--N), and soluble reactive phosphorus (SRP) were analyzed according to the protocol of Aminot and Chaussepied (1983) described in Baumgarten et al. (1996)

within 48 h after the collection. We followed the protocol suggested by Strickland and Parsons (1972), described in Baumgarten et al. (1996), to determine ammoniacal-N (NH_3—N + NH_4^+—N) within 24 h after collection. Dissolved inorganic nitrogen (DIN) was obtained by the sum of nitrite, nitrate and ammoniacal-N. The retained particulate materials on the filters were frozen at −20 °C for a subsequent spectrophotometric determination of chlorophyll *a* and phaeophytin *a* using extraction in 90% acetone (method 10200-H, Rice et al., 2012). Aliquots (300 mL) of the water samples were filtered through a 0.45-μm-pore-size mixed cellulose ester membrane (47 mm diameter, HATF, Millipore, Billerica, USA) and analyzed according to Aminot and Chaussepied (1983), described in Baumgarten et al. (1996), to measure dissolved silica. Total suspended solids (TSS) were determined gravimetrically by weighing pre-combusted filters of 1.2-μm pore-size glass-fiber (47 mm diameter, type APFC, Millipore, Billerica, USA) used for water sample filtration according to Rice et al. (2012) (methods 2540D). Part of the unfiltered water samples was used to quantify total nitrogen (TN) and total phosphorus (TP) according to Valderrama (1981), described in UNESCO (1983). All the laboratory analysis were performed in triplicate.

2.4. Hydrological data

2.4.1. Water budget

The estuarine water budget was calculated to evaluate the hydrological regime. The budget assumes that the system volume (V in m^3) does not change in time (t in s), which is a valid assumption for time scales between weeks and a couple of years. Based on the principle of mass (or volume) conservation, for any water volume that enters the estuary, an equivalent volume must exit at the same rate, or $dV/dt = 0$. The net water budget can be written as:

$$dV/dt = V_P + V_E + V_G + V_Q + V_H + V_R \quad (1)$$

where V_P represents the precipitation flux onto the estuary surface and shrimp farms pounds (surface areas of 1.7 and 7.2 km^2, respectively). It is calculated by the direct product of the precipitation rate (in m s^{-1}) and surface area (in m^2), and it is positive, which represents a water input. V_E represents the evaporation flux from the estuary surface and is calculated similarly as V_P whereas it is negative as it represents a water output. Daily data of precipitation and evaporation were obtained from the Brazilian National Institute of Meteorology (INMET) in the Jaguaruana meteorological station (#OMM:82493) located approximately 40 km away from the study area. The data were reduced to monthly means (Table 1, Fig. 2). V_G represents the groundwater flux and was assumed to be zero (Kjerfve et al., 1996). V_Q represents the surface runoff from the drainage basin. The water budget of the drainage basin was calculated as:

$$V_Q = [(P - ET)\ kA - V_I] / t \quad (2)$$

where P is the precipitation rate, ET is the evapotranspiration rate (in m s^{-1}), and A is the drainage area (4250 km^2). We used the ET values calculated for the Jaguaribe basin by Gondim et al. (2010). Surface runoff only exists if the precipitation rate is greater than the evapotranspiration rate, and after the soil becomes saturated with rain. Therefore, it is necessary to include the runoff ratio coefficient (k) that represents the fraction of the precipitation in the runoff. This coefficient ranges between 0.5 and 0.8 for Brazilian semi-arid soils (Cavalcanti, 2010) and we used a mean value of 0.65. The second term of the right side of equation (2) stands for the volume impounded in reservoirs (V_I). The semi-aridity requires the water impoundment as much as possible during the short rainy period. Therefore, most of the initial water surplus is trapped in reservoirs. The largest reservoirs in the Piranji catchment are Macacos and Batente with a joint capacity of 44 hm^3 (FUNCEME/COGERH, 2018). There are several other smaller reservoirs; however, owing to the lack of inventory, we estimated the total impounded capacity as 75 hm^3, based on the reservoirs surface area. The term V_H in equation (1) represents the direct human-induced water flux such as water transfer, groundwater pumping, and wastewater production. In small estuaries located in large urban areas, the wastewater contribution can be higher than all other factors (Schettini et al., 2016, 2017). However, the human population in the estuary margins is very small, and this factor is negligible. Finally, the term V_R represents the residual flow required to maintain dV/dt = 0.

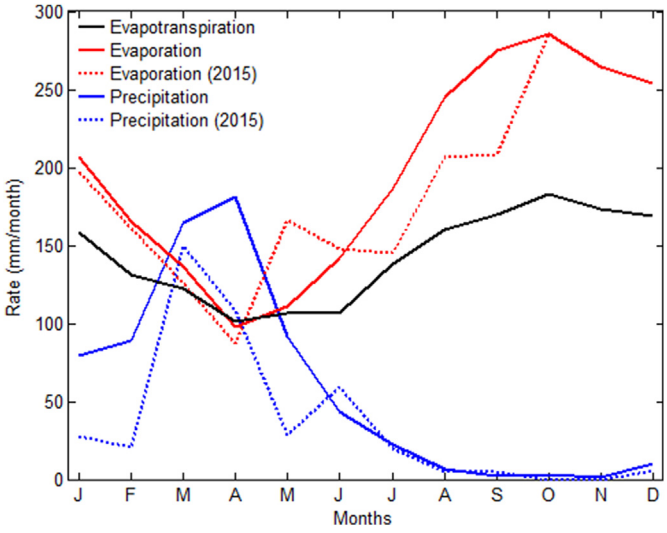

Fig. 2. Monthly mean values of evapotranspiration, evaporation, and precipitation in the study area (Source: the Brazilian National Institute of Meteorology).

Table 1
Values of the estuary water flow and the components of the water budget due to continental runoff (V_Q), precipitation (V_P), evaporation (V_E) and residual (V_R). Positive and negative values represent inflow and outflow, respectively. All values are in $m^3\ s^{-1}$.

Month (2015)	V_Q	V_P	V_E	V_R
February	0.000	0.075	−0.594	0.520
April	7.350	0.370	−0.300	−7.420
June	0.000	0.204	−0.507	0.300
August	0.000	0.016	−0.687	0.670
October	0.000	0.000	−0.949	0.950
December	0.000	0.019	−0.844	0.820

2.4.2. Salt balance

The mass balance of salt was based on the methodology proposed by Land-Ocean Interactions in the Coastal Zone (LOICZ) (Gordon et al., 1996). The salt balance in the system was estimated using the water budget, and calculated as:

$$V * dS/dt = V_R * S_R + V_X (S_2 - S_1) \quad (3)$$

which considers the main salt fluxes (evaporation, residual and mixture with coastal waters), where S1 and S2 correspond to the salinity of estuary and ocean, respectively. Residual salinity (S_R) is the average of S1 and S2. For S1 and S2 we used the mean values from sub-surface and bottom obtained at St1 and St3, respectively. St1 and St3 were the upstream and downstream compartments of the estuary under greater influence of river and coastal waters, respectively. Water exchange flux between estuary and ocean, V_X, was estimated as:

$$V_X = V_R * S_R/(S_1 - S_2) \quad (4)$$

In 2015, the Piranji estuary was marked by an unusual hydrological condition in which a hyposaline system (salinity 9.4) was observed in April and hypersaline in February and from August to December (mean

Table 2
Values of the water fluxes used for calculating the salt balance. The rainy period corresponds to April and the dry period covers February, August, October and December 2015. Positive and negative values represent inflow and outflow, respectively. All values are in $m^3\ s^{-1}$.

Period	V_Q	V_P	V_E	V_R
Rainy	7.350	0.370	−0.300	−7.420
Dry	0.000	0.027	0.768	0.740

of salinity: 51.1) with a transition period in June (salinity 35.9). Thus, the salt balance was calculated for the rainy period (April) and for the dry period (February and August to December). The transition period (June) was excluded in the calculation. Table 2 indicates the water fluxes used in the measurement.

2.5. Statistical analyses

Significant differences ($p < 0.05$) between the surface and bottom samples were tested using a Mann–Whitney *U* test for each variable. Correlations between parameters were examined by calculating the Spearman rank correlation coefficient (ρ). Non-parametric tests were used because, as determined by Shapiro–Wilk tests, most variables were not normally distributed, except temperature, pH, TP and TSS. The variation of environmental data and phytoplankton pigments was analyzed by principal component analysis (PCA) and cluster analysis.

Before running the PCA, we tested the Spearman correlations (ρ) between all the variables considering the whole data set (Supplementary Table S2). Afterwards we excluded some highly correlated variables to run the PCA. The variables: euphotic zone depth (Zeu), saturation oxygen (SO), phaeophytin and SRP were excluded because of their strong correlations with Secchi depth, dissolved oxygen (DO), chlorophyll *a* and TP, respectively. For nitrogen, only DIN was used because of its correlation with Nitrate, Nitrite and Ammoniacal-N. Lastly, temperature was excluded due to its small intra-annual variation. Even performing this procedure, we chose to maintain some variables significantly correlated in PCA because their exclusion could result in the loss of relevant information to depict the environmental variation from the studied system. The Kaiser–Meyer–Olkin (KMO) test was used to measure the sample adequacy, and Bartlett's test of sphericity was applied to verify the applicability of PCA.

The significance of grouping in the cluster analysis was tested using similarity profile test (SIMPROF). The data were transformed by log(x + 1) for all analyses, except the pH, which is already in logarithmic scale. The Paleontological statistics software package (PAST) v. 2.12 (Hammer et al., 2001) was used for PCA and PRIMER v. 6.0 (Clarke and Gorley, 2006) was used for cluster analysis and SIMPROF. Statistica 7 was used for Spearman test and Mann–Whitney *U* test. KMO test and Bartlett's test were conducted using R (R Development Core Team, 2014).

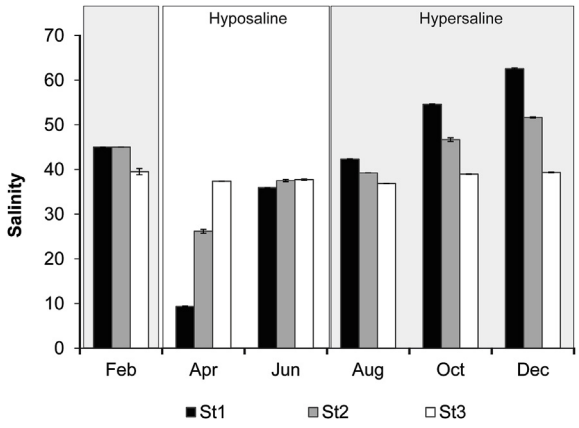

Fig. 3. Mean values of salinity throughout 2015 in the Piranji estuary measured from station 1 (St1), station 2 (St2) and station 3 (St3). The error bars indicate standard deviations.

3. Results

3.1. Physicochemical environment

Physical and chemical parameters measured in the Piranji estuary exhibited no significant differences between the surface and bottom for most of the variables (Mann-Whitney, $p > 0.05$) whereas the Dissolved oxygen concentrations (DO) and Saturation oxygen (SO) values were significantly different ($p < 0.05$). Therefore, data were presented as mean ± standard deviation from surface and bottom measures for all variables, except for DO and SO (Supplementary Table S1).

The Piranji estuary presented a hyposaline regime in the middle (April) and at the end of the rainy period (June), as can be noted by the salinity levels rising from upstream (St1) to downstream (St3) (Fig. 3). The slight hyposaline regime at the end of the rainy period (June) indicated a transition to the hypersaline regime, which was found throughout the dry period and even at the beginning of the rainy period (February). That is, the salinity of the estuary was higher than the surrounding coastal waters. The hypersalinity condition was intensified as the dry season progressed and peaked (62.6 ± 0.17) at the end of the hydrological deficit period in the upstream estuary (St1).

Throughout the year, the temperature varied from 25.6 to 29.0 °C throughout the estuary with values increasing from downstream to upstream. The euphotic zone (Z_{eu}) increased from St1 to St3 whereas the total suspended solids (TSS) decreased from St1 to St3. Particularly at St1, TSS values peaked in the middle (October) and end of the dry period (December). The measured pH values varied very little during all year, and the estuarine waters were mostly alkaline. Regarding oxygen, the differences between surface and bottom were more evident at St1 with little variation at St3. Oxygen levels at St3 reached higher values than at St1 and St2, and were frequently consistent with undersaturation. These results (maximum depth, euphotic zone, temperature, pH, total suspended solids, dissolved oxygen, and oxygen saturation) are summarized in Supplementary Table S1.

3.2. Nutrients

All nutrients (DIN, TN, Si, SRP, and TP) indicated a clear spatial gradient with higher concentrations upstream (St1) and lower concentrations downstream (St3) (Fig. 4). St3 indicated low concentrations for all nutrients during the year. In most samples (except for St1 in October and December when nitrite prevailed), ammoniacal-N comprised more than 70% of DIN (Fig. 5).

Among all stations, the highest DIN concentrations were found in April when the estuary received the highest precipitation and was hyposaline. At St1, the DIN amount started to reduce markedly in October whereas the other stations were more stable temporally apart from the peak in April (Fig. 4a). Regarding the temporal variation of TN, the lowest concentrations for St1 and St2 occurred at the beginning of the dry period (August) whereas the highest concentrations occurred at the end of same period (December) (Fig. 4b).

Total phosphorus presented a shallower gradient, and reached higher values in October (Fig. 4c) when the estuary was hypersaline. However, SRP concentrations were higher in August, and reached the lowest amounts in October. At St1, SRP concentrations increased continuously from February when the estuary was still hypersaline to June and August, and then started to decline in October and stayed reduced during rest of the hypersaline period (December). At St2 and St3, temporal variations of SRP were less pronounced (Fig. 4d).

A spatial variation was not clear in DIN:SRP ratios, but there was only a temporal variation with higher ratios in the rainy season and

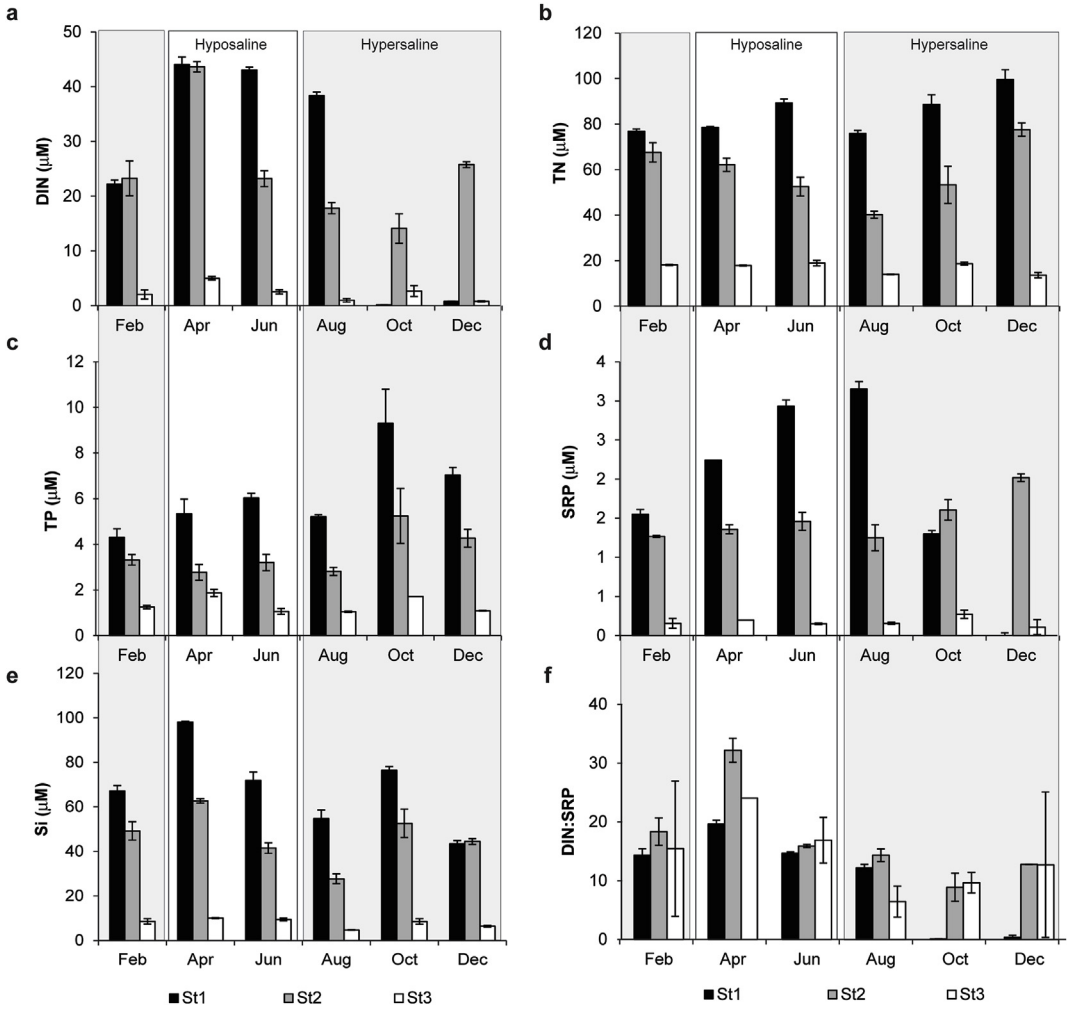

Fig. 4. Mean values and standard deviations of (a) dissolved inorganic nitrogen (DIN), (b) total nitrogen (TN), (c) total phosphorous (TP), (d) soluble reactive phosphorous (SRP), (e) dissolved silica (Si) and (f) DIN:SRP ratio throughout 2015 in the Piranji estuary. St1: station 1; St2: station 2; St3: station 3.

smaller ratios in the dry period (Fig. 4e). Particularly at St1, such ratio fell sharply during October and December together with the sharp decreases in DIN.

Regarding dissolved Silica, the spatial pattern of decreasing concentrations from upstream to downstream was very pronounced, as with TN. Temporally, concentrations peaked in April at all stations, followed by a decline beginning in June and extended through August. Then, the concentrations rose again in October (Fig. 4f).

3.3. Total phytoplankton biomass (TPB)

TPB indicated a spatial gradient with a trend similar to nutrients,

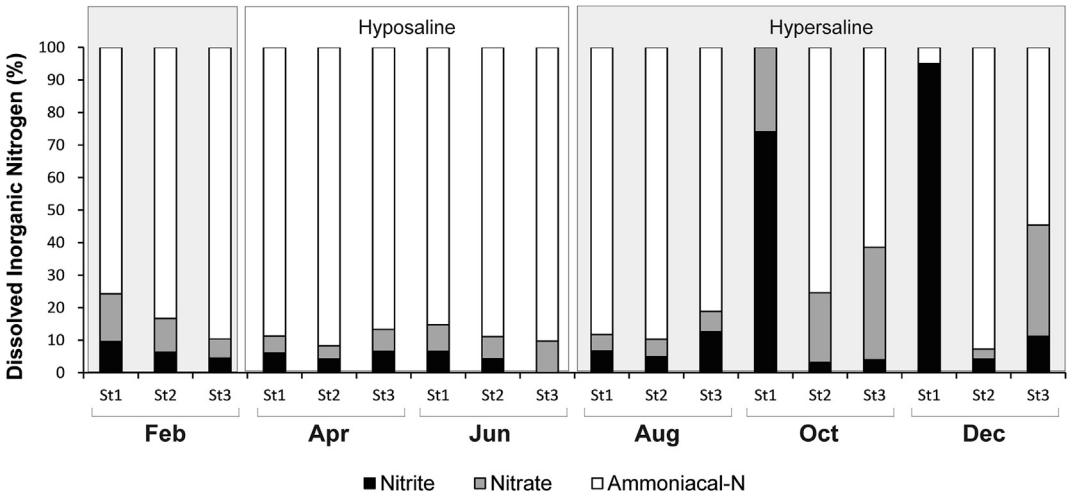

Fig. 5. Mean values from each form of dissolved inorganic nitrogen throughout 2015 in the Piranji estuary.

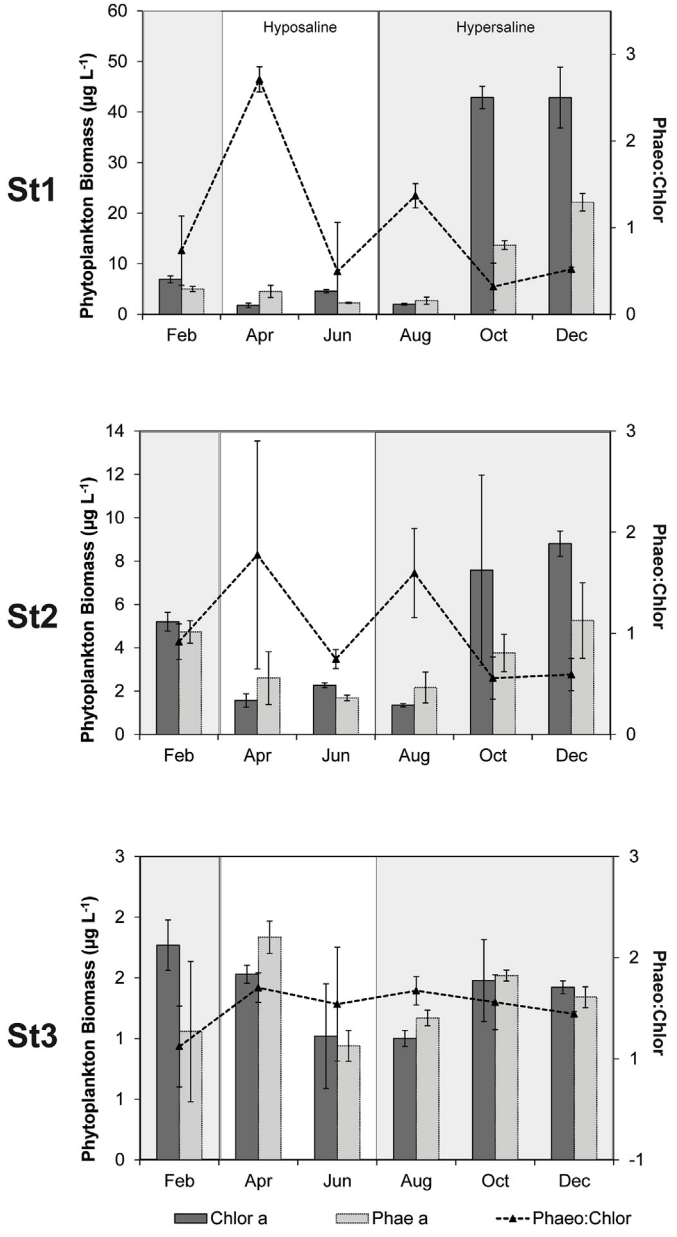

Fig. 6. Mean values and standard deviation of chlorophyll *a*, phaeophytin *a* and phaeophytin *a*: chlorophyll *a* ratio in St1, St2 and St3 throughout 2015 in the Piranji estuary.

and decreased from St1 to St3 (Fig. 6). Temporally, an intra-annual variation could be noted at St1 and St2 where the TPB was initially very low at the beginning of the dry period but then greatly increased (about 4–20 times) in October and December. In the rainy season, TPB was very low, and reached minimum concentrations in April. Near the estuary mouth (St3), TPB was very low and stable throughout the year.

Based on Phaeo:Chlor ratio, the most stressful conditions were during April and August when pigment degradation prevailed above the active chlorophyll *a*. In the other months, such ratios were < 1 at St1 and St2 which indicated less stressful conditions for the phytoplankton biomass (Fig. 6).

3.4. Annual and spatial variation of physicochemical parameters and phytoplankton biomass

The Kaiser-Meyer-Olkin (KMO > 0.5) and Bartlett's sphericity ($p < 0.05$) tests showed that the samples met the criteria for PCA ordination. In the PCA, the two first axes explained 73.8% of the total variation of environmental data (Fig. 7). Axis 1 (39.8%) was negatively correlated with Secchi depth (r = −0.76) and DIN:SRP ratio (r = −0.61), and positively correlated with TN (r = 0.88), TP (r = 0.94), Si (r = 0.78), TSS (r = 0.75) and chlorophyll *a* (r = 0.89). Axis 2 (34.0%) was negatively correlated with salinity (r = −0.76), pH (r = −0.47) and dissolved oxygen (r = −0.90) but positively correlated with DIN (r = 0.87), Phaeo:Chlor ratio (r = 0.73) and DIN:SRP ratio (r = 0.67).

Based on the differences between physicochemical variables among the three sampling stations throughout the year, four distinctive and significant groups ($p < 0.05$) were revealed by cluster analysis and the SIMPROF test (Supplementary Fig. S1) as displayed in the PCA (Fig. 7). Regarding how such clusters distributed on the factorial plane of PCA, it can be observed that group I was more related to higher Secchi depth and lower nutrients concentrations. Moreover, the lack of significant temporal differences among samples from St3 was responsible for grouping them in group I.

Group II formed by St1 samples in October and December was positioned at the axis 1 extreme part and was distinctive from the other groups by the highest values of pH, salinity, chlorophyll *a* and TSS. Group III encompassed most of the St1 and St2 samples and was related to the higher values of nutrients (especially TN, TP, and Si). Finally, Group IV included St1 and St2 samples during April and can be distinguished by high concentrations of DIN, high DIN:SRP and Phaeo:Chlor ratios, and lower values of pH, salinity, and dissolved oxygen.

3.5. Estuary behavior during hyposaline and hypersaline regimes

Based on the salinity profile throughout the year, the estuary indicated two regimes: a hyposaline period followed by a brief transition (slightly hyposaline) and hypersaline-dominant-regime during the rest of the year (Section 3.1). Considering only the months when hyposaline (April) and slightly hyposaline conditions were present (June), significant positive correlations were found between the salinity and Z_{eu} ($\rho = 0.90$), SO ($\rho = 0.83$) and pH ($\rho = 0.83$) (Spearman test, $p < 0.05$). Moreover, significant inverse correlations were found between the salinity and DIN ($\rho = -0.83$) and phaeophytin *a* ($\rho = -0.94$) (Spearman test, $p < 0.05$). Significant positive correlations were also detected between chlorophyll *a* and SRP ($\rho = 0.94$) and TP ($\rho = 0.94$) (Spearman test, $p < 0.05$) (Supplementary Table S3).

However, during hypersaline conditions, significant positive correlations were found between the salinity and temperature ($\rho = 0.68$), TN ($\rho = 0.87$), SRP ($\rho = 0.70$), TP ($\rho = 0.86$), Si ($\rho = 0.70$), chlorophyll *a* ($\rho = 0.97$) and phaeophytin *a* ($\rho = 0.89$) (Spearman test, $p < 0.05$). Moreover, a significant inverse correlation between the salinity and Z_{eu} was found ($\rho = -0.68$). Chlorophyll *a* also indicated significant positive correlations with temperature ($\rho = 0.66$), TN ($\rho = 0.88$), SRP ($\rho = 0.69$), TP ($\rho = 0.88$), Si ($\rho = 0.75$) and phaeophytin *a* ($\rho = 0.88$); and there was a significant negative correlation with Z_{eu} ($\rho = -0.73$) (Supplementary Table S4).

3.6. Water and salt balances

The water and salt fluxes during 2015 were estimated as presented in Table 3. The evaporation drove the water budget during the dry period (Fig. 8a) with a net loss to the atmosphere of -64×10^3 m^3/day. This loss would be compensated by an equivalent water inflow from the coastal sea (V_R). This volume inflow transported salt into the systems (2.9×10^6 kg/day) by advection. However, considering the system in steady state and the salt conservation, the same amount of salt must exit the system by dispersion. This result implies a water exchange volume of $V_X = 249.9 \times 10^3$ m^3/day. The ratio between the system volume to the sum of V_X and V_R give us the flushing time of 13.5 days. During the rainy period the river flow drove the water budget

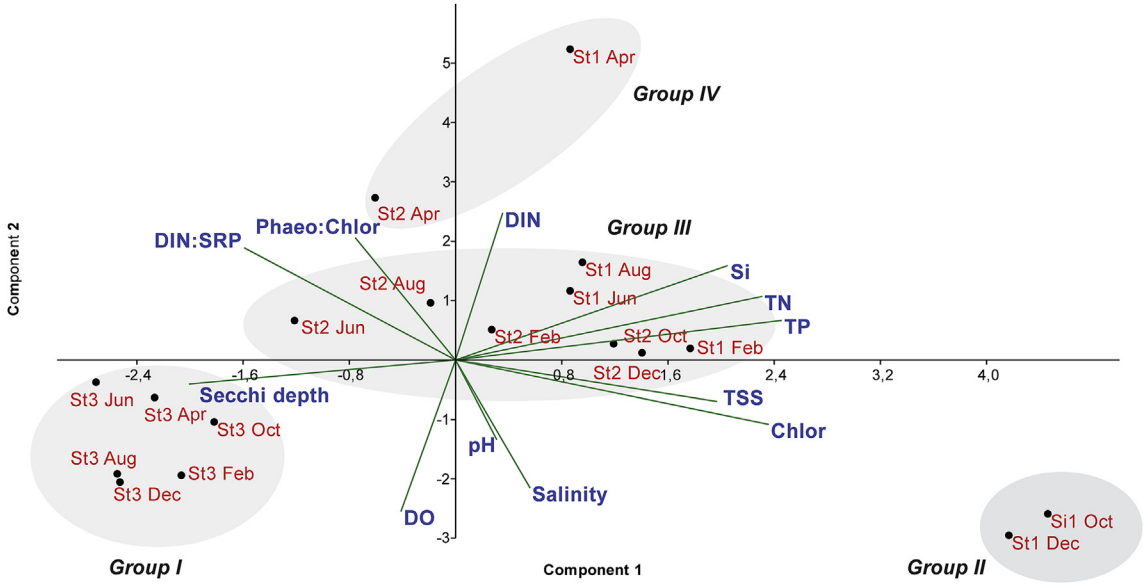

Fig. 7. Principal component analysis (PCA) indicating the pattern of orientation based on the intra-annual variability of environmental variables and nutrient concentrations throughout 2015 in the Piranji estuary. Groups I to IV were significant ($p < 0.05$) and extracted by cluster analysis and SIMPROF test.

Table 3
Data used for the water and salt budgets calculations. Positive values mean flow into the system, whereas negative values mean flow out the system.

System Characteristics		
Area (km^2)	1.70	
Length (km)	25.00	
Average depth (m)	2.50	
Volume ($10^3\ m^3$)	4250.00	
Water fluxes	**Rainy Period**	**Dry Period**
V_Q ($10^3\ m^3$/d)	635.00	0.00
V_P ($10^3\ m^3$/d)	32.00	2.00
V_E ($10^3\ m^3$/d)	−26.00	−66.00
V_R ($10^3\ m^3$/d)	−641.00	+64.00
Salt balance		
Estuary salinity	9.36	51.10
Ocean salinity	37.40	39.50
$V_R.S_R$ (10^3 kg/d)	−14,986.60	+2899.20
V_X ($10^3\ m^3$/d)	534.50	249.90
$\tau_{hydraulic\ residence}$ (d)	6.60	66.40
$\tau_{Flushing}$ (d)	3.60	13.50

(Fig. 8b) when the water inflow was $641 \times 10^3\ m^3$/day with an equivalent outflow to the coastal sea (V_R), advection of 15×10^6 kg/day of salt, a volume exchange (V_X) of $534.5 \times 10^3\ m^3$/d is required. These values give a flushing time of 3.6 days. The flushing time estimates are for the lower part of the estuary, where the samples were taken, and will increase considering the whole system.

4. Discussion

In this study, we evaluated the intra-annual variations of physico-chemical parameters, nutrients, and chlorophyll *a* (TPB) in an estuary faced with extreme climate duality and the interaction of these factors with each other to understand the processes controlling nutrient concentrations and phytoplankton biomass. Based on the longitudinal salinity gradient along the continuum — upstream (St1) to downstream (St3) — observed along the year, the estuary presented two distinct hydrological conditions: a shorter one with freshwater inflow leading to hyposaline distribution, and a longer one with low inflow of freshwater leading to hypersaline distribution. Those periods were marked by considerable differences in precipitation, evaporation and flushing time that resulted in noticeable variations in the salinity profiles, nutrient concentrations, and phytoplankton biomass.

No significant variations in water temperature and vertical salinity profiles were observed during this study, indicating that the Piranji estuary behaved as a well mixed system (Schettini et al., 2017), which implies that tides are the main driver of the hydrodynamics at short time-scales. Compared to several other estuaries, the Piranji estuary is short and shallow, and its relatively small size makes it more susceptible to climate and anthropogenic changes; these consequences were evident mainly in salinity, suspended solids and TPB.

Most of the time, salinity was similar to or greater than the adjacent marine coastal waters with a landward increase. April and June were the only exceptions, when salinity increased towards the sea. Evaporation drove the water budget throughout the dry season leading to salt inflow and dominance of hypersalinity in the Piranji estuary. This phenomenon was also observed at the beginning of the rainy period, when evaporation was still higher than precipitation. Although February corresponded to the beginning of the rainy season in 2015, conditions still reflected those from the end of the dry season of 2014. The period between 2010 and 2016 was particularly harsh in the region owing to an extreme reduction in precipitation, leading to what is claimed as being one of the longest and most intense droughts in decades in the semi-arid Northeast Brazil region (Marengo et al., 2017b). Our study was performed in 2015, during a severe drought, although a previous assessment in the Piranji estuary also reported hypersaline conditions (Schettini et al., 2017), and it is likely this situation is a long-term feature, at least seasonally. The area now occupied by shrimp farms was previously occupied by salt extraction pounds since the early 20th century, thus supporting this assumption. However, it is important to note that the decrease in precipitation and river discharge in years of severe drought may be a factor that increases the hypersalinity levels in the estuary, or even extend the time that the system remains under the hypersaline regime along the year.

We hypothesized that the freshwater input would provide adequate conditions for the development of the phytoplankton during the rainy season whereas the primary productivity would be reduced in the dry (unfavorable) season. That is, the phytoplankton might take advantage of the relief from the hypersalinity. However, we observed the opposite trend with a high-duality salinity pattern, with a hyposaline regime

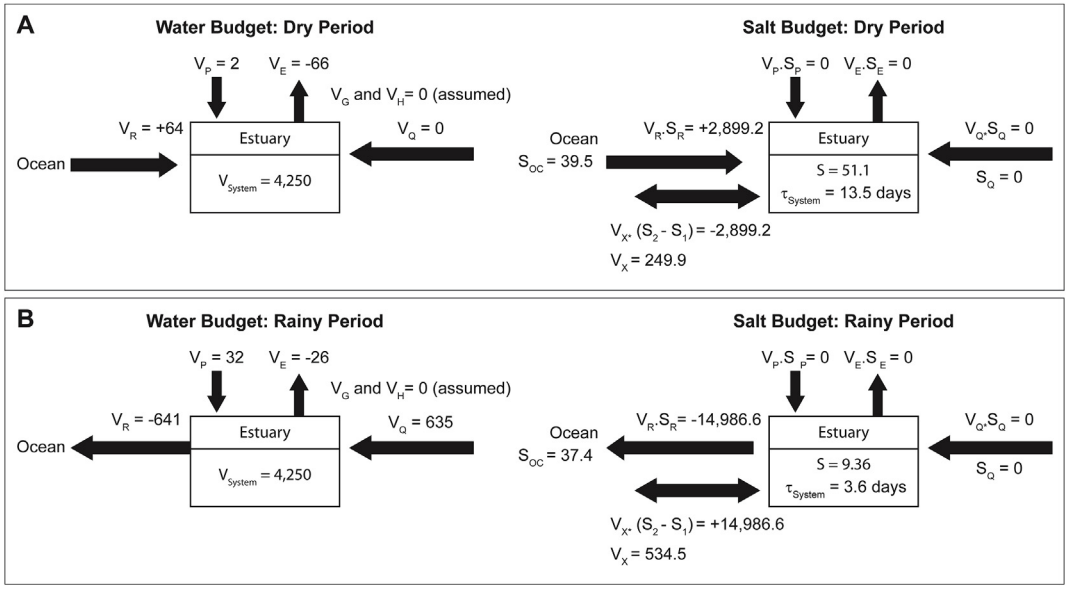

Fig. 8. Water and salt budgets for the dry (a) and rainy (b) periods. System volume (V_{Syst}) in 10^3 m^3; water flows (V_P, V_E, V_Q, V_R, detailed in Section 2.4) in 10^3 m^3/d; salinity (S) in PSU (~kg/m^3); salt fluxes in kg/d. V_P = flow of water by precipitation, V_E = evaporation flow, V_Q = riverine discharge, V_R = residual flow; V_G = groundwater flow; V_X = flow of water exchange. Positive values indicate input to the system whereas negative values indicate system output.

lasting from April to June and a hypersaline regime dominating the rest of the year. In such conditions, the rainy season acted as an unfavorable season. The change to a hypersaline regime regulating the phytoplankton biomass and most nutrients dynamics was more pronounced at St1.

On the other hand, St3 was much more influenced by coastal waters. It presented higher water transparency, lower nutrients and stable phytoplankton biomass throughout the year with little influence of riverine inputs. The spatial gradient from St1 to St3 and the low intra-annual variation in biotic and abiotic variables on this downstream zone are likely to be related to the absence of high-flow events that could promote significant changes on lower estuary (Saeck et al., 2013; Chowdhury et al., 2017).

Under-saturation levels of oxygen were observed most of the year and especially in April except for the TPB peak during the edge of the dry season. These results could indicate the occurrence of net heterotrophy, already observed in other estuaries, such as the Mandovi-Zuari estuarine system (Ram et al., 2003), Cochin estuary (Thottathil et al., 2008) and Godavari estuary (Sarma et al., 2009). Net heterotrophy indicates the respiration dominance over primary production due to organic matter input from freshwater inflow (Ram et al., 2003).

TPB exhibited positive correlations with salinity and most nutrients (TN, SRP, TP, and Si) and a negative correlation with Z_{eu} due to phytoplankton shading during the hypersaline regime. In turn, TPB was closely related to SRP and TP when the estuary was hyposaline. This means that while in the hyposaline regime phosphorus appears to be a significant driver of TPB concentrations, in the hypersaline regime the phytoplankton growth is related to all nutrients. These positive correlations reflect the spatial variation along the salinity gradient in both regimes, in which higher nutrients and TPB were always greater upstream. Additionally, these findings indicate a bottom-up control of the temporal variation of TPB (Saeck et al., 2013; Buck et al., 2014).

However, is important to note that SRP concentrations during hyposaline regime were higher than that found in hypersaline conditions, suggesting that other factors prevented a larger uptake of this nutrient by the phytoplankton and a consequent upstream TPB accumulation. Often, the limiting factors to phytoplankton associated with rainfall increase are reduced water residence time and lower light availability (Saeck et al., 2013), which appears to be our study case.

The TPB exhibited the lowest concentration in April. On the one hand, freshwater flow can carry nutrients into estuaries and consequently increase their concentrations and availability for phytoplankton (Barroso et al., 2016), whereas on the other hand flow events also decrease water residence time and increase the turbidity (Lancelot and Muylaert, 2011; Tirok and Scharler, 2013). Therefore, in tropical estuaries, either an increase or a decrease in phytoplankton biomass can occur in the rainy season (Barroso et al., 2016).

The Zeu/Zmax ratio in April was lowest in the upstream zone (Supplementary Table S1), indicating a higher potential for light limitation in the rainy period due to the increased risk of phytoplankton cells sinking out of euphotic zone, leading to a loss of TPB (Lu and Gan, 2015), given that the estuary was well mixed. In the rainy period, the presence of more stressful conditions for phytoplankton growth and greater cell senescence were indicated by high Phaeo:Chlor ratios (Taguchi et al., 1993) observed at St1 and St2 in April. Once a higher phaeophytin concentration can be also a result of intense grazing pressure on phytoplankton (Taguchi et al., 1993), the role of the temporal dynamics of zooplankton on regulating this community by a top-down control cannot be discounted (Carrasco and Perissinotto, 2012) and should also be investigated.

In turn, in the hypersaline regime, St1 and St2 presented pronounced levels of TPB during October and December when salinity reached maximum levels (up to 63) and water residence time was high. The peaks in TPB at high salinities were recorded in other hypersaline estuaries (Bettarel et al., 2011; Muir and Perissinotto, 2011). The combined effects of the higher water residence time (Lancelot and Muylaert, 2011; Tirok and Scharler, 2013) and efficient nutrient uptake rates by phytoplankton (du Plooy et al., 2014; Hemraj et al., 2017) could explain such an increase under hypersaline conditions as well as the depletion of DIN (on October and December) and SRP (on December).

Our results for an hypersaline estuary were consistent with those found in positive estuaries, as the TPB peak occurred during the season of higher water residence time (Saeck et al., 2013; Lu and Gan, 2015; Geyer et al. 2018), independent of the salinity (up to 63). The TPB peak at St1 during the hypersaline period suggests the salinity was not sufficiently high to cause osmotic stress capable of causing a crash in the phytoplankton community, at least concerning total biomass. An analogous situation was found in Coorong estuary (Australia), where the increase in water residence time benefited the local phytoplankton

community, despite the salinity being up to 72 (Jendyk et al., 2014). Other studies performed in Coorong observed that chlorophyll *a* started to decrease at salinity levels > 107, suggesting that the local phytoplankton community can tolerate a wider range of salinity (Leterme et al., 2015). However, this rise in TPB under hypersaline condition often occurs due to an increase in dominance of few species tolerant to salinity, including harmful algae (Jendyk et al., 2014; Nche-Fambo et al., 2015; Kang et al., 2015; Hemraj et al., 2017). These cases corroborate our findings, indicating that a longer flushing time would favor TPB even at moderate hypersaline conditions. However, the role of salinity on phytoplankton biodiversity must still be carefully evaluated.

It is important to note that dissolved silica peaked in April and October. The first peak in the rainy period has been previously observed in positive tropical estuaries when they receive higher freshwater inputs (Sarma et al., 2010; Subha Anand et al., 2014). However, the peak observed in October could be related to long water residence times that also could led to Si build-up by retention (Largier et al., 1997). In addition, since the freshwater was not the source of Si in the dry season, recycling of biogenic silica could also explain its increase as shown in the Elbe estuary (Germany) during prolonged residence times (Amann et al., 2014). Additionally, the peak of non-siliceous species of phytoplankton in October cannot be ruled out as a further explanation to Si build-up, and should still be evaluated.

The TP peak in October (in all stations) could also be associated with sediment resuspension and retention due to a high water residence time. Anthropogenic inputs are also an additional P source as the site has been intensively occupied by shrimp farms (Schettini et al., 2017). Moreover, SRP values were comparable to those in other tropical estuaries subjected to anthropogenic impacts that may be caused by shrimp farms (such as the Jaguaribe estuary in northeast Brazil) (Eschrique et al., 2008) and agricultural or domestic effluent discharge (such as the Godavari estuary in India) (Sarma et al., 2010). Although even the highest SRP levels in the Piranji estuary were lower than that observed in heavily polluted tropical estuaries (Guenther et al., 2015), it is difficult to affirm whether the estuary is under low anthropogenic impact or whether the system is resistant owing to P retention in sediments (Wang and Li, 2010). In the lower estuary, SRP concentrations were within the range of coastal waters from northeast Brazil (Bastos et al., 2011).

Nitrogen dynamics were also related to salinity with TN and DIN decreasing towards the sea. DIN indicated a clear peak in April which was negatively correlated with salinity, and possibly associated with the increased river discharge as previously reported (Silva et al., 2015). In most of the stations, throughout the year, ammoniacal-N accounted 50–90% of DIN and reached higher concentrations at St1 and St2. Particularly at St1, ammoniacal-N suffered an intense decrease during October and December, possibly related to the phytoplankton biomass. Ammoniacal-N can have anthropogenic sources and result of biological excretion and organic matter regeneration by bacterial activity (Bhavya et al., 2016). However, undersaturated levels of oxygen may prevent the efficient conversion from ammoniacal-N to nitrite and nitrate by bacteria (nitrification) (Molnar et al., 2013). A significant inverse Spearman correlation was found between DIN (50–90% ammoniacal-N) and oxygen both in hyposaline and hypersaline periods (Supplementary Tables S3 and S4, respectively). Ammoniacal-N can also be produced by dissimilatory nitrate reduction to ammonium (DNRA) (Giblin et al., 2013) which is important to reduce nitrate and to conserve input nitrogen as NH_4^+ (biologically preferred form of N) (Reynolds, 2006) in the system (Molnar et al., 2013; Cao et al., 2016). The observed ammoniacal-N enrichment is comparable with concentrations found in tropical eutrophic estuaries such as the Cachoeira estuary in northeast Brazil (Silva et al., 2015) and the Cochin estuary in India (Bhavya et al., 2016). Only at St1 were the concentrations below the limit of detection, possibly due to phytoplankton assimilation in October and December. Other processes could be also related to DIN decrease such as denitrification (reduces NO_3^- and NO_2^- to N_2 and N_2O) and anaerobic ammonium oxidation (Anammox; $NH_4^+ + NO_2^- \rightarrow N_2$) (Burgin and Hamilton, 2007). Particularly at St2, the decline in DIN was accompanied by a decline in TN, which suggests that nitrogen was removed.

Concerning the DIN:SRP ratios, elevated values were obtained in April which was consistent with the higher freshwater ratios in comparison to marine waters (Howarth and Marino, 2006). The sharp decline at St1 in October and December was possibly caused by the phytoplankton bloom which is an active component in determining the water stoichiometry (Deutsch and Weber, 2012). This event occurs by nutrient uptake leading to N or P depletion in the water (Arrigo, 2005). Therefore, the elevated phytoplankton (persistent from October to December) must have been sustained by species strongly adapted to living in a low DIN:SRP ratio and fast-growing.

Small estuaries are usually neglected, and not only scientifically, despite being locally important since they support local populations and fishing resources. They can also sustain planktonic communities adapted to face rapid environmental changes, such as the shift from hypo-to hypersalinity. The unusual condition of these estuaries highlights the importance of our study as a model to understand the behavior of relatively small tropical estuaries under the influence of a semi-arid climate with respect to intra-annual and spatial dynamics of nutrients and total phytoplankton biomass. Further studies should identify the species of the phytoplankton community and the other components of the planktonic trophic web. Considering prevalent climate change, increases are predicted in the frequency and intensity of droughts and salinity in estuaries. Their effects on phytoplankton community (richness and dominance) may be critical for the survival of this ecosystem and need to be better understood.

5. Conclusions

In this semi-arid estuary, rainfall rather than drought stood out as a disturbance for phytoplankton biomass. The changes in the water balances (from a short fluvial discharge to a long evaporation and high water residence time) had striking effects on phytoplankton biomass and nutrient dynamics marked by a phytoplankton bloom during the water shortage season.

Acknowledgements

This work was supported by the Cearense Foundation for Scientific and Technological Development Support (FUNCAP) (BFP Program); the Coordination for the Improvement of Higher Education Personnel (CAPES) (PNPD fellowship for HSB) and the National Council for Scientific and Technological Development (CNPq) (233808/2014-0, 404290/2016-7 and 307061/2017).

Appendix A. Supplementary data

Supplementary data related to this article can be found at https://doi.org/10.1016/j.ecss.2018.08.023.

References

Amann, T., Weiss, A., Hartmann, J., 2014. Silica fluxes in the inner Elbe estuary, Germany. Biogeochemistry 118, 389–412. https://doi.org/10.1007/s10533-013-9940-3.

Aminot, A., Chaussepied, M., 1983. Manuel des Analyses Chimiques en Milieu Marin. Centre National pour l'Exploration des Oceans, Brest.

Arrigo, K.R., 2005. Marine microorganisms and global nutrient cycles. Nature 437, 349–355. https://doi.org/10.1038/nature04159.

Azhikodan, G., Yokoyama, K., 2016. Spatio-temporal variability of phytoplankton (Chlorophyll-a) in relation to salinity, suspended sediment concentration, and light intensity in a macrotidal estuary. Continent. Shelf Res. 126, 15–26. https://doi.org/10.1016/j.csr.2016.07.006.

Barroso, H. de S., Becker, H., Melo, V.M.M., 2016. Influence of river discharge on phytoplankton structure and nutrient concentrations in four tropical semi-arid estuaries. Braz. J. Oceanogr. 64, 37–48. https://doi.org/10.1590/S1679-87592016101406401.

Bastos, R.B., Feitosa, F.A.N., Koening, M.L., Machado, R.C.A., Muniz, K., 2011. Caracterização de uma zona costeira tropical (Ipojuca-Pernambuco-Brasil): produtividade fitoplanctônica e outras variáveis ambientais. Braz. J. Aquat. Sci. Technol. 15, 1–10. https://doi.org/10.14210/bjast.v15n1.p1-10.

Bauer, J.E., Cai, W.-J., Raymond, P.A., Bianchi, T.S., Hopkinson, C.S., Regnier, P.A.G., 2013. The changing carbon cycle of the coastal ocean. Nature 504, 61–70. https://doi.org/10.1038/nature12857.

Baumgarten, M.G.Z., Rocha, J.M.B., Niencheski, L.F.H., 1996. Manual de análises em oceanografia química. Editora FURG, Rio Grande.

Bettarel, Y., Bouvier, T., Bouvier, C., Carré, C., Desnues, A., Domaizon, I., Jacquet, S., Robin, A., Sime-Ngando, T., 2011. Ecological traits of planktonic viruses and prokaryotes along a full-salinity gradient. FEMS Microbiol. Ecol. 76, 360–372. https://doi.org/10.1111/j.1574-6941.2011.01054.x.

Bhavya, P.S., Kumar, S., Gupta, G.V.M., Sudheesh, V., Sudharma, K.V., Varrier, D.S., Dhanya, K.R., Saravanane, N., 2016. Nitrogen uptake dynamics in a tropical eutrophic estuary (Cochin, India) and adjacent coastal waters. Estuar. Coast 39, 54–67. https://doi.org/10.1007/s12237-015-9982-y.

Buck, C.M., Wilkerson, F.P., Parker, A.E., Dugdale, R.C., 2014. The influence of coastal nutrients on phytoplankton productivity in a shallow low inflow estuary, Drakes Estero, California (USA). Estuar. Coast 37, 847–863. https://doi.org/10.1007/s12237-013-9737-6.

Burgin, A.J., Hamilton, S.K., 2007. Have we overemphasized the role of denitrification in aquatic ecosystems ? A review of nitrate removal pathways. Front. Ecol. Environ. 5, 89–96. https://doi.org/10.1890/1540-9295(2007)5[89:HWOTRO]2.0.CO;2.

Campos, J.N.B., Studart, T.M.C., 2003. Climatologia - diagnóstico ambiental (Org.) In: Campos, A.A. (Ed.), A zona costeira do Ceará: diagnóstico para a gestão integrada. Aquasis, Fortaleza, pp. 51–54.

Cao, W., Yang, J., Li, Y., Liu, B., Wang, F., Chang, C., 2016. Dissimilatory nitrate reduction to ammonium conserves nitrogen in anthropogenically affected subtropical mangrove sediments in Southeast China. Mar. Pollut. Bull. 110, 155–161. https://doi.org/10.1016/j.marpolbul.2016.06.068.

Carrasco, N.K., Perissinotto, R., 2012. Development of a halotolerant community in the St. Lucia estuary (South Africa) during a hypersaline phase. PLoS One 7, 1–14. https://doi.org/10.1371/journal.pone.0029927.

Cavalcanti, N.B., 2010. Efeito do escoamento da água de chuva em diferentes coberturas. Engenharia Ambiental – Espirito Santo do Pinhal 7, 201–210.

Chowdhury, M., Hardikar, R., Kesavan, H.C., Thomas, J., Mitra, A., Rokade, M.A., Naidu, V.S., Sukumaran, S., 2017. Nutrient stoichiometry and freshwater flow in shaping of phytoplankton population in a tropical monsoonal estuary (Kundalika Estuary). Estuar. Coast Shelf Sci. 198, 73–91. https://doi.org/10.1016/j.ecss.2017.08.019.

Clarke, K.R., Gorley, R.N., 2006. PRIMER v6: User Manual/Tutorial. PRIMER-E Ltd., Plymouth Marine Laboratory, Plymouth.

Cloern, J.E., Abreu, P.C., Carstensen, J., Chauvaud, L., Elmgren, R., Grall, J., Greening, H., Johansson, J.O.R., Kahru, M., Sherwood, E.T., Xu, J., Yin, K., 2016. Human activities and climate variability drive fast-paced change across the world's estuarine-coastal ecosystems. Global Change Biol. 22, 513–529. https://doi.org/10.1111/gcb.13059.

Cole, G.A., 1983. Textbook of Limnology, third ed. Waveland Press, Long Grove.

Costanza, R., de Groot, R., Sutton, P., van der Ploeg, S., Anderson, S.J., Kubiszewski, I., Farber, S., Turner, R.K., 2014. Changes in the global value of ecosystem services. Global Environ. Change 26, 152–158. https://doi.org/10.1016/j.gloenvcha.2014.04.002.

Deutsch, C., Weber, T., 2012. Nutrient ratios as a tracer and driver of ocean biogeochemistry. Annu. Rev. Mar. Sci. 4, 113–141. https://doi.org/10.1146/annurev-marine-120709-142821.

du Plooy, S., Smit, A., Perissinotto, R., Muir, D., 2014. Nitrogen uptake dynamics of a persistent cyanobacterium Cyanothece sp. bloom in Lake St Lucia, South Africa. Afr. J. Mar. Sci. 36, 155–161. https://doi.org/10.2989/1814232X.2014.922124.

Eschrique, S.A., Marins, R.V., Moreira, M.O.P., Almeida, M.D., 2008. Hidrogeoquímica do Fósforo no Estuário do Jaguaribe (CE) (Org.) In: Braga, E.S. (Ed.), Volume Especial do IIISBO: Oceanografia e Mudanças Globais. 1. Instituto Oceanográfico da Universidade de São Paulo, São Paulo, pp. 629–647.

Frota, F.F., Paiva, B.P., Schettini, C.A.F., 2013. Intra-tidal variation of stratification in a semi-arid estuary under the impact of flow regulation. Braz. J. Oceanogr. 61, 23–33. https://doi.org/10.1590/S1679-87592013000100003.

FUNCEME/COGERH, 2018. Portal Hidrológico Do Ceará. http://www.hidro.ce.gov.br/, Accessed date: 4 August 2018.

Geyer, N.L., Huettel, M., Wetz, M.S., 2018. Phytoplankton spatial variability in the river-dominated estuary, Apalachicola Bay, Florida. Estuar. Coast. https://doi.org/10.1007/s12237-018-0402-y.

Giblin, A.E., Tobias, C.R., Song, B., Weston, N., Banta, G.T., Rivera-Monroy, H., R H, V., 2013. The importance of dissimilatory nitrate reduction to ammonium (DNRA) in the nitrogen cycle of coastal ecosystems. Oceanography 26, 124–131. https://doi.org/10.5670/oceanog.2013.54.

Godoy, M.D.P., Lacerda, L.D. de, 2015. Mangroves response to climate change: a review of recent findings on mangrove extension and distribution. An Acad. Bras Ciências 87, 651–667. https://doi.org/10.1590/0001-3765201520150055.

Gondim, R.S., Fuck Jr., S.C.F., Maia, A.H.N., Evangelista, S.R.M., 2010. Balanço hídrico na bacia do Jaguaribe, Ceará, utilizando evapotranspiração de referência Penman-Monteith FAO estimada com dados mínimos. Fortaleza, Embrapa, Boletim de Pesquisa e Desenvolvimento. No 36, 48p.

Gordon Jr., D.C., Boudreau, P., Mann, K.H., Ong, J.-E., Silvert, W., Smith, S.V., Wattayakorn, G., Wulff, F., Yanagi, T., 1996. LOICZ Biogeochemical Modelling Guidelines, vol. 96 LOICZ, Den BurgTexel.

Guenther, M., Araújo, M., Flores-Montes, M., Gonzalez-Rodriguez, E., Neumann-Leitão, S., 2015. Eutrophication effects on phytoplankton size-fractioned biomass and production at a tropical estuary. Mar. Pollut. Bull. 91, 537–547. https://doi.org/10.1016/j.marpolbul.2014.09.048.

Hammer, Ø., Harper, D.A.T., Ryan, P.D., 2001. Past: paleontological statistics software package for education and data analysis. Paleontol Electron 4 (1), 1–9.

Hemraj, D.A., Hossain, M.A., Ye, Q., Qin, J.G., Leterme, S.C., 2017. Plankton bioindicators of environmental conditions in coastal lagoons. Estuar. Coast Shelf Sci. 184, 102–114. https://doi.org/10.1016/j.ecss.2016.10.045.

Howarth, R.W., Marino, R., 2006. Nitrogen as the limiting nutrient for eutrophication in coastal marine ecosystems: evolving views over three decades. Limnol. Oceanogr. 51 (1), 364–376. https://doi.org/10.4319/lo.2006.51.1_part_2.0364.

IPCC, 2014. https://www.ipcc.ch/pdf/assessment-report/ar5/syr/AR5_SYR_FINAL_SPM.pdf, Accessed date: 30 September 2017.

Jendyk, J., Hemraj, D.A., Brown, M.H., Ellis, A.V., Leterme, S.C., 2014. Environmental variability and phytoplankton dynamics in a South Australian inverse estuary. Continent. Shelf Res. 91, 134–144. https://doi.org/10.1016/j.csr.2014.08.009.

Kang, Y., Koch, F., Gobler, C.J., 2015. The interactive roles of nutrient loading and zooplankton grazing in facilitating the expansion of harmful algal blooms caused by the pelagophyte, *Aureoumbra lagunensis*, to the Indian River Lagoon, FL, USA. Harmful Algae 49, 162–173. https://doi.org/10.1016/j.hal.2015.09.005.

Kjerfve, B., Schettini, C.A.F., Knoppers, B., Lessa, G., Ferreira, H.O., 1996. Hydrology and Salt Balance in a Large, Hypersaline Coastal Lagoon: Lagoa de Araruama, Brazil. Estuar. Coast Shelf Sci. 42, 701–725. https://doi.org/10.1006/ecss.1996.0045.

Lancelot, C., Muylaert, K., 2011. Trends in estuarine phytoplankton ecology. In: In: Wolanski, E. (Ed.), Treatise on Estuarine and Coastal Science, Functioning Ecosystems at the Land-ocean Interface, vol. 7. pp. 5e15. https://doi.org/10.1016/B978-0-12-374711-2.00703-8.

Largier, J., 2010. Low-inflow estuaries: hypersaline, inverse, and thermal scenarios. In: Valle-Levinson, A. (Ed.), Contemporary Issues in Estuarine Physics. Cambridge University Press, New York, pp. 247–272.

Largier, J.L., Hollibaugh, J.T., Smith, S.V., 1997. Seasonally hypersaline estuaries in mediterranean-climate regions. Estuar. Coast Shelf Sci. 45, 789–797. https://doi.org/10.1006/ecss.1997.0279.

Leterme, S.C., Allais, L., Jendyk, J., Hemraj, D.A., Newton, K., Mitchell, J., Shanafield, M., 2015. Drought conditions and recovery in the Coorong wetland, South Australia in 1997–2013. Estuar. Coast Shelf Sci. 163, 175–184. https://doi.org/10.1016/j.ecss.2015.06.009.

Lu, Z., Gan, J., 2015. Controls of seasonal variability of phytoplankton blooms in the Pearl River Estuary. Deep Sea Res. Part II Top. Stud. Oceanogr. 117, 86–96. https://doi.org/10.1016/j.dsr2.2013.12.011.

Marengo, J.A., Torres, R.R., Alves, L.M., 2017a. Drought in Northeast Brazil—past, present, and future. Theor. Appl. Climatol. 129, 1189–1200. https://doi.org/10.1007/s00704-016-1840-8.

Marengo, J.A., Alves, L.M., Alvala, R.C., Cunha, A.P., Brito, S., Moraes, O.L.L., 2017b. Climatic characteristics of the 2010-2016 drought in the semi-arid Northeast Brazil region. An Acad. Bras Ciências 1–13. https://doi.org/10.1590/0001-3765201720170206.

Meireles, A.J.A., Cassola, R.S., Tupinambá, V.S., Queiroz, L.D.S., 2007. Impactos ambientais decorrentes das atividades da carcinicultura ao longo do litoral cearense, nordeste do Brasil. Mercator-Revista de Geografia da UFC 6, 83–105.

Molisani, M.M., Cruz, A.L.V., Maia, L.P., 2006. Estimation of the freshwater river discharge to estuaries in.Ceará State. Arquivos de Ciências do Mar 39, 53–60.

Molnar, N., Welsh, D.T., Marchand, C., Deborde, J., Meziane, T., 2013. Impacts of shrimp farm effluent on water quality, benthic metabolism and N-dynamics in a mangrove forest (New Caledonia). Estuar. Coast Shelf Sci. 117, 12–21. https://doi.org/10.1016/j.ecss.2012.07.012.

Muir, D.G., Perissinotto, R., 2011. Persistent phytoplankton bloom in lake St. Lucia (iSimangaliso wetland park, South Africa) caused by a cyanobacterium closely associated with the genus *Cyanothece* (*Synechococcaceae, Chroococcales*). Appl. Environ. Microbiol. 77 (17), 5888–5896. https://doi.org/10.1128/AEM.00460-11.

Nche-Fambo, F.A., Scharler, U.M., Tirok, K., 2015. Resilience of estuarine phytoplankton and their temporal variability along salinity gradients during drought and hypersalinity. Estuar. Coast Shelf Sci. 158, 40–52. https://doi.org/10.1016/j.ecss.2015.03.011.

Pereira-Filho, J., Schettini, C.A.F., Rörig, L., Siegle, E., 2001. Intratidal variation and net transport of dissolved inorganic nutrients, POC and chlorophyll a in the Camboriú river estuary, Brazil. Estuar. Coast Shelf Sci. 53, 249–257. https://doi.org/10.1006/ecss.2001.0782.

R Development Core Team, 2014. R: a Language and Environment for Statistical Computing. R Foundation for Statistical Computing, Vienna, Austria3-900051-07-0. http://www.R-project.org/.

Ram, A.S., Nair, S., Chandramohan, D., 2003. Seasonal shift in net ecosystem production in a tropical estuary. Limnol. Oceanogr. 48, 1601–1607. https://doi.org/10.4319/lo.2003.48.4.1601.

Reynolds, C.S., 2006. The Ecology of Phytoplankton. Cambridge University Press.

Rice, E.W., Baird, R.B., Eaton, A.D., Clesceri, L.S., 2012. Standard Methods for the Examination of Water and Wastewater, twenty-second ed. American Public Health Association, American Water Works Association, Water Environment Federation.

Robins, P.E., Skov, M.W., Lewis, M.J., Giménez, L., Davies, A.G., Malham, S.K., Neill, S.P., McDonald, J.E., Whitton, T.A., Jackson, S.E., Jago, C.F., 2016. Impact of climate change on UK estuaries: a review of past trends and potential projections. Estuar. Coast Shelf Sci. 169, 119–135. https://doi.org/10.1016/j.ecss.2015.12.016.

Saeck, E.A., Hadwen, W.L., Rissik, D., O'Brien, K.R., Burford, M.A., 2013. Flow events drive patterns of phytoplankton distribution along a river–estuary–bay continuum. Mar. Freshw. Res. 64, 655–670. https://doi.org/10.1071/MF12227.

Santos, C.A.C., Brito, J.I.B., 2007. Análise dos índices de extremos para o semi-áridodo Brasil e suas relações com TSM e IVDN. Revista Brasileira de Meteorologia 22, 303–312.

Sarma, V.V.S.S., Gupta, S.N.M., Babu, P.V.R., Acharyya, T., Harikrishnachari, N., Vishnuvardhan, K., Rao, N.S., Reddy, N.P.C., Sarma, V.V., Sadhuram, Y., Murty, T.V.R., Kumar, M.D., 2009. Influence of river discharge on plankton metabolic rates in the tropical monsoon driven Godavari estuary, India. Estuar. Coast Shelf Sci. 85, 515–524. https://doi.org/10.1016/j.ecss.2009.09.003.

Sarma, V.V.S.S., Prasad, V.R., Kumar, B.S.K., Rajeev, K., Devi, B.M.M., Reddy, N.P.C., Sarma, V.V., Kumar, M.D., 2010. Intra-annual variability in nutrients in the Godavari estuary, India. Continent. Shelf Res. 30, 2005–2014. https://doi.org/10.1016/j.csr.2010.10.001.

Schettini, C.A.F., Miranda, J.B., Valle-Levinson, A., Truccolo, E.C., 2016. The circulation of the lower Capibaribe estuary (Brazil) and its implications for the transport of scalars. Braz. J. Oceanogr. 64, 263–276. https://doi.org/10.1590/S1679-87592016119106403.

Schettini, C.A.F., Valle-Levinson, A., Truccolo, E.C., 2017. Circulation and transport in short, low-inflow estuaries under anthropogenic stresses. Reg. Stud. Mar. Sci. 10, 52–64. https://doi.org/10.1016/j.rsma.2017.01.004.

Silva, M.A.M., Souza, M.F.L., Abreu, P.C., 2015. Spatial and temporal variation of dissolved inorganic nutrients, and chlorophyll a in a tropical estuary in Northeastern Brazil: dynamics of nutrient removal. Braz. J. Oceanogr. 63, 1–15. https://doi.org/10.1590/S1679-87592015064506301.

Strickland, J.D.H., Parsons, T.R., 1972. A Practical Handbook of Seawater Analysis. Bulletin of the Fisheries Research Board of Canada, Ottawa.

Subha Anand, S., Sardessai, S., Muthukumar, C., Mangalaa, K.R., Sundar, D., Parab, S.G., Dileep Kumar, M., 2014. Intra- and inter-seasonal variability of nutrients in a tropical monsoonal estuary (Zuari, India). Continent. Shelf Res. 82, 9–30. https://doi.org/10.1016/j.csr.2014.04.005.

Taguchi, S., Laws, E.A., Bidigare, R.R., 1993. Temporal variability in chlorophyll a and phaeopigment concentrations during incubations in the absence of grazers. Mar. Ecol. Prog. Ser. 101, 45.

Thottathil, S.D., Balachandran, K.K., Gupta, G.V.M., Madhu, N.V., Nair, S., 2008. Influence of allochthonous input on autotrophic–heterotrophic switch-over in shallow waters of a tropical estuary (Cochin Estuary), India. Estuar. Coast Shelf Sci. 78, 551–562. https://doi.org/10.1016/j.ecss.2008.01.018.

Tirok, K., Scharler, U.M., 2013. Dynamics of pelagic and benthic microalgae during drought conditions in a shallow estuarine lake (Lake St. Lucia). Estuar. Coast Shelf Sci. 118, 86–96. https://doi.org/10.1016/j.ecss.2012.12.023.

Uddin, M.S., de Ruyter van Steveninck, E., Stuip, M., Shah, M.A.R., 2013. Economic valuation of provisioning and cultural services of a protected mangrove ecosystem: a case study on Sundarbans Reserve Forest, Bangladesh. Ecosys. Serv. 5, 88–93. https://doi.org/10.1016/j.ecoser.2013.07.002.

UNESCO, 1983. Chemical Methods for Use in marine Environmental Monitoring (Manual and guides, 12). Intergovernmental Oceanographic Commission. http://www.jodc.go.jp/info/ioc_doc/Manual/055950eo.pdf, Accessed date: 10 October 2016.

Uvo, C.R.B., Berndtsson, R., 1996. Regionalization and spatial properties of Ceará state rainfall in Notrheast Brazil. J. Geophys. Res. 101 (D2), 4221–4433. https://doi.org/10.1029/95JD03235.

Valderrama, J.C., 1981. The simultaneous analysis of total nitrogen and total phosphorus in natural waters. Mar. Chem. 10, 109–122. https://doi.org/10.1016/0304-4203(81)90027-X.

Valle-Levinson, A., Schettini, C.A.F., 2016. Fortnightly switching of residual flow drivers in a tropical semiarid estuary. Estuar. Coast Shelf Sci. 169, 46–55. https://doi.org/10.1016/j.ecss.2015.12.008.

Wang, Q., Li, Y., 2010. Phosphorus adsorption and desorption behavior on sediments of different origins. J. Soils Sediments 10, 1159–1173. https://doi.org/10.1007/s11368-010-0211-9.